Steel and Composite Structures, *Vol. 32, No. 5 (2019) 671-686*
DOI: https://doi.org/10.12989/scs.2019.32.5.671

Active control to reduce the vibration amplitude of the solar honeycomb sandwich panels with CNTRC facesheets using piezoelectric patch sensor and actuator

Amir Amini [2], M. Mohammadimehr[*1] and A.R. Faraji [2]

[1] *Department of Solid Mechanics, Faculty of Mechanical Engineering, University of Kashan, Kashan, Iran*
[2] *Department of Control, Faculty of Computer and Electrical Engineering, University of Kashan, Kashan, Iran*

(*Received April 22, 2019, Revised June 13, 2019, Accepted June 15, 2019*)

Abstract. Active control of solar panels with honeycomb core and carbon nanotube reinforced composite (CNTRC) facesheets for smart structures using piezoelectric patch sensor and actuator to reduce the amplitude of vibration is a lack of the previous study and it is the novelty of this research. Of active control elements are piezoelectric patches which act as sensors and actuators in many systems. Their low power consumption is worth mentioning. Thus, deriving a simple and efficient model of piezoelectric patch's elastic, electrical, and elastoelectric properties would be of much significance. In the present study, first, to reduce vibrations in composite plates reinforced by carbon nanotubes, motion equations were obtained by the extended rule of mixture. Second, to simulate the equations of the system, up to 36 mode shape vectors were considered so that the stress strain behavior of the panel and extent of displacement are thoroughly evaluated. Then, to have a more acceptable analysis, the effects of external disturbances (Aerodynamic forces) and lumped mass are investigated on the stability of the system. Finally, elastoelectric effects are examined in piezoelectric patches. The results of the present research can be used for micro-vibration suppression in satellites such as solar panels, space telescopes, and interferometers and also to optimize active control panel for various applications.

Keywords: active vibration control; solar panels; piezoelectric patches; honeycomb core; CNTRC

1. Introduction

Nowadays, the issue of suppressing micro-vibration levels in sandwich panels owing to their effect on the sensitive sensors measuring in low frequencies is of great importance. The reason lies in the fact that even the presence of the lowest amplitude vibrations generated by solar radiation, aerodynamic forces will significantly increase measurement errors in optical instruments or microgravity experiments, where the microvibrations are resulted from the operation of other equipment required for correct functioning (e.g., reaction wheels). Thus, it is vital to control the micro vibrations to a certain amount by active control procedures such as piezoelectric patches (Sharma *et al*. 2015, Xu *et al*. 2018b). A great number of studied have been conducted some of which are mentioned as follows:

Applying a flywheel actuator for flexible spacecraft vibration suppression and attitude maneuvers, Xu *et al*. (2018a) obtained a system model by the Euler-Lagrange methodology and the assumed mode method.

A novel sandwich panel which is named RC panel-Helical springs-RC panel (RHR) sandwich panel was proposed by Rashad *et al*. (2019). Tahouneh (2017) aimed at filling the gap in the area about vibration analysis of multiwalled carbon nanotubes (MWCNTs) curved panels by providing 3-D vibration analysis results for functionally graded multiwalled carbon nanotubes (FG-MWCNTs) sandwich structure with power-law distribution of nanotube. Nasihatgozar *et al*. (2017) used higher order shear deformation theory to deal with general equations of motion for free vibration analysis response of thick three-layer doubly curved sandwich panels (DCSP) under simply supported boundary conditions (BCs). Mohammadimehr *et al*. (2018b) presented free vibration analysis of magneto-electro-elastic cylindrical composite panel reinforced by various distributions of carbon nanotubes (CNTs) with considering open and closed circuits boundary conditions based on first-order shear deformation theory (FSDT).

Some researchers worked about free vibration analysis of functionally graded (FG)-carbon nanotubes reinforced composite (CNTRC) sandwich beam (Mohammadimehr *et al*. 2017c, Mohammdimehr and Shahedi 2017), micro porous cylindrical shell (Yazdani *et al*. 2019), annular sandwich plate using Ritz method (Emdadi *et al*. 2019), sandwich thick plate (Mohammadimehr *et al*. 2016b), nano rods (Mohammadimehr and Rahmati 2013).

Do *et al*. (2017) presented role of material combination and new numerical results of mechanical behavior for functionally graded (FG) sandwich plates in high temperature. They concluded that a strong impact of severe high temperature affected the mechanical behaviors of sandwich plates and also, the material combinations play a crucial role and significantly on the mechanical behaviors

*Corresponding author, Associate Professor,
E-mail: mmohammadimehr@kashanu.ac.ir

ISSN: 1229-9367 (Print), 1598-6233 (Online)

of sandwich plates. Bui *et al*. (2013) considered dynamic analysis of sandwich beams with FG core using a truly meshfree radial point interpolation method. They used a truly meshfree RPIM using Cartesian transformation method and employed the effective core properties using rule of mixture or Mori-Tanaka methods. Also, they considered penalty method to treat the material discontinuities. Also, the other works studied stability of double-walled carbon nanotubes (DWCNTs) (Arani *et al*. 2011), stability of micro sandwich shell conveying fluid flow using DQM (Mohammadimehr and Mehrabi 2017).

A boundary control strategy was proposed by He *et al*. (2018) to control the vibrations of two flexible wings. Using Hamilton's principle, they established the system dynamic model which consisted of governing equations, i.e., four partial differential equations and boundary conditions, and several ordinary differential equations.

As the most widely used algorithm for noise control, Filtered-x least mean square (FxLMS) was assumed by Niu *et al*. (2019) to control adaptive noise and vibrations. However, the secondary path identified offline was not able to distinguish the system characteristics in real-time which made the classical FxLMS inapplicable for time-varying system. To solve this problem, a new method for online modeling of secondary path was proposed, i.e., it was realized by the existing signals.

In a new study, the analysis of an adaptive backstepping fuzzy sliding mode control approximating the unknown system dynamics for a cantilever beam was carried out by Fang *et al*. (2018). They came to the conclusion that the adaptive backstepping fuzzy sliding mode control was derived from the combination of the backstepping method and adaptive fuzzy strategy.

A computationally efficient method was proposed by Daraji *et al*. (2017) to identify the optimal placement of sensor/actuator (s/a) pairs for active vibration control of a flexible structure. Dynamically symmetric and asymmetric structures under external force and structure base excitations were examined by this method so that the optimal distribution would be determined based on time-frequency responses analysis.

Kumar and Narayanan (2008) examined the optimal placement of collocated piezoelectric actuator/sensor pairs on flexible beams by a model-based linear quadratic regulator (LQR) controller. They used a finite element method based on Euler–Bernoulli beam theory and formulated the optimal location of actuator and sensor for different boundary conditions. In another study, Chhabr *et al*. (2011) considered the active vibration control of cantilever beam like structures with the laminated piezoelectric sensor and actuator layers bonded on top and bottom surfaces of the beam. A finite element model based on Euler-Bernoulli beam theory was developed in their study. They presented a design of state/output feedback control by Pole placement technique and LQR optimal control approach to achieve the optimal control. Lin and Cao (2018) investigated the control strategies based on the displacement feedback and LQR method. These strategies were applied by pasting the piezoelectric material on the surface of the plate structure. Based on the Hamilton principle and applying the first-order piston theory to describe the aerodynamic loads, the governing equation of the plate system with the piezoelectric actuator was derived.

To determine the type of controller, an accurate dynamic model of the system that consist of sandwich panel, piezoelectric patches and lumped mass, is required that can be obtained by the use of Hamilton's principle. High-order shear deformation theory and high-order sandwich panel theory are methods for investigating a lumped mass on the composite plate in based on Hamiltonian principle (Daouadji *et al*. 2016, Zenkour and Aljadani 2018).

Using smart structures consisting of composite and sandwich panel has been increased considerably due to high strength and rigidity. One of the most important reasons for using these structures is the possibility of taking advantages of piezoelectric layers. They are usually made of three parts; top and bottom face sheets, a foam or honeycomb core. Faces are generally made of high strength materials, whereas the core layer is made of a low specific weight material. So, the flexibility of the core is more than the facesheet (Nguyen *et al*. 2015, Mohammadimehr *et al*. 2017b).

Arani and Kiani (2018) presented nonlinear free and forced vibration analysis of microbeams resting on the nonlinear orthotropic visco-Pasternak foundation with different boundary conditions. Ö mer Gündoğdu studied vibration behavior of honeycomb sandwich composites filled with polyurethane foam by Taguchi Method. Kumar *et al*. (2019) investigated instability and Vibration analyses of FG cylindrical panels under parabolic axial compressions. Mohammadimehr *et al*. (2018a) considered bending, buckling, and free Vibration analyses of carbon nanotube reinforced composite beams and experimental tensile test to obtain the mechanical properties of nanocomposite. Nguyen and Tran (2018) illustrated free Vibration of tapered BFGM beams using an efficient shear deformable finite element model.

In the present study, to improve the bending and strain behavior of solar panels, the sandwich layer is assumed with a honeycomb homogenous core composed of the 5052 aluminum alloy and composite face sheets reinforced by carbon nanotube which play an important role in low weight and stiffness of the structure (Selim *et al*. 2017). The considerable mechanical properties by carbon nanotubes (CNTs) have attracted much attention because of the elastic modulus and tensile strength of CNTs reinforced microcomposite are much harder and stronger than steel, while the much lighter. The CNTs reinforced composite have many applications in various fields such as electromechanical devices, microsensors, biosensors, aerospace and shipping. Symmetric and un-symmetric distributions of nanotubes are considered for facesheets of sandwich microplates such as uniform distribution and various functionally graded distributions. Material properties of sandwich microplates are obtained by the extended rule of mixture (Shen and Xiang 2012).

However, for piezoelectric patches, it is important that a more accurate analysis be done on their physical and electrical properties and their equations be obtained in the base of Ritz functions (Aglietti *et al*. 1997). (Aglietti *et al.*

2002) utilized the Lagrange equations to derive a very compact mathematical model of an electromechanical system comprised of a sandwich panel equipped with mass loaded panel and piezoelectric patches which act as sensors and actuators. The results of simulations were in concurrence with finite element method.

Based on the dynamic analysis of the system and pole placement, a simple controller such as the second order linear regression can be used to control the behavior of the system to obtain admissible vibration frequency amplitude (Nadirian *et al*. 2017, Lin and Cao 2018). The robustness of the system can also be assessed and analyzed taking into account uncertainties such as variations in the weight of the lumped mass and the position of disturbance force.

Micro-vibration suppression in satellites particularly in their solar panels which are largely subjected to solar radiation and aerodynamic forces is of much significance. These micro-vibrations cause shear and flexural stresses in sandwich panel's arm and fault in satellite performance in the long run. Therefore, it's necessary to keep them lower than a specific level. To do so, employing local controllers which perform independently of the satellite control system can be a very useful and effective.

Active control of solar panels with honeycomb core and carbon nanotube reinforced composite facesheets for smart structures using sensor and actuator to reduce the amplitude of vibration is a lack of the previous study and it is the novelty of this research. The results of this research can be used to optimize active control panel for various applications. In the present study, the mechanical properties of carbon nanotube reinforced composite facesheets and the honeycomb core are first obtained by the extended rule of mixture, and then, the dynamic equations of the system are derived using the Lagrange relations based on the principle of minimum potential energy. With a linear relation based on vibration mode shape, system equation will be solved in state space. Also, stability of the system has been evaluated against mass and position variations of the lumped mass, position variations of the disturbance force, and the position replacement of the piezoelectric sensor patch with that of the actuator patch. Sandwich panel frequency in extremum point against variations in core-to-face sheet thickness ratio and the displacements of the sandwich panel and aluminum plate are analyzed in detail. Finally, the possibility of vibrations reaching an optimum level is proved by linear quadratic regression controller.

2. Material properties of CNTs reinforced composite facesheets and sandwich panel core

Sandwich panels are composed of a homogenous aluminum honeycomb core and two carbon nanotubes reinforced composite (CNTRC) facesheets with different weight percentages of CNT. The sandwich panel with length a, width b, and thickness h is shown in Fig. 1. As seen, the core is of thickness h_c and CNTRC facesheets of thickness h_f $(h = h_c + h_f)$.

The dynamic equations of the system have been obtained based on the following assumptions (Marynowski 2012):

- Compared to the facesheets, the core is both thicker and softer.
- No slipping takes at the interfaces between the core and facesheets.
- Full bond exists between the core and facesheets. Thus, the displacement between the core and the top facesheet $z = +h_c/2$ is the same as the one in the bottom facesheet in $z = -h_c/2$.

In the Cartesian coordinate system, the origin point is assumed to be in the center of the core and one of the corners of the cube (Fig. 1). The extended rule of mixture (Mohammadimehr *et al*. 2016a), which is a simple and convenient way to estimate the material properties of the two-phase composites, is written as follows (Rajabi *et al*. 2019)

$$E_{11} = \eta_1 V_{NT}^{t,b} E_{11NT} + V_M E_{11M} \tag{1a}$$

$$\frac{\eta_2}{E_{12}} = \frac{V_{NT}^{t,b}}{E_{22NT}} + \frac{V_M}{E_{22M}} \tag{1b}$$

$$\frac{\eta_3}{G_{12}} = \frac{V_{NT}^{t,b}}{G_{12NT}} + \frac{V_M}{G_M} \tag{1c}$$

$$\upsilon_{12} = V_{NT}^{t,b} \upsilon_{12NT} + V_m \upsilon_M \tag{1d}$$

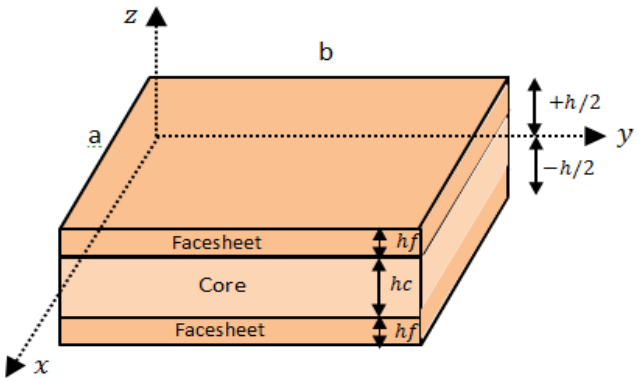

Fig. 1 A schematic view of sandwich panel with homogenous core and CNTRC facesheets

$$\rho = V_{NT}^{t,b}\rho_{NT} + V_m\rho_M \quad (1e)$$

where the subscripts *NT* and *M* denote the nanotube and the matrix, respectively. As seen above, the top and bottom facesheets are shown by *t* and *b*, respectively. $V_{NT} + V_M = 1$ is obtained as the relation for the composites. In the above relations, $\eta i\ (i = 1, 2, 3)$ is considered as the efficiency parameter and *v* is Poisson's ratio. Furthermore, E_{11}, E_{22} and *G* represent longitudinal, transversely elastic moduli, and shear modulus, respectively. The efficiency parameters are defined numerically for CNTs and can be obtained by molecular dynamics simulations (Han and Elliott 2007).

3. System description and constitutive equations

3.1 The effect of masses on the solar panel

Of the equipment mounted on the solar panel are sensors, actuators, and telecommunication equipment. The equipment is modeled as lumped masses and the disturbances as point forces (Fig. 2). The schematic diagram of the Cartesian coordinate system on the solar panel can be seen in Fig. 3.

As seen in Fig. 2, twin patches of piezoelectric material have been employed on the panel with one pair acting as sensors and another as actuators. The reason for using this structure is to bond the outer connectors from the control unit. Any variations in displacement are detected by the sensors which, depending contraction or expansion of the patch, induce an electric field and send it to the control unit. The control unit, in turn, sends the actuators a voltage to independently control any vibration on the sandwich panel (Malekzadeh *et al*. 2012).

3.2 Constitutive equations

First, the classical displacement field for the sandwich plate is expressed as (Mohammadimehr *et al*. 2017a)

$$\begin{cases} U(x,y,z,t) = u(x,y,t) - z\dfrac{\partial w(x,y,t)}{\partial x} \\ V(x,y,z,t) = v(x,y,t) - z\dfrac{\partial w(x,y,t)}{\partial x} \\ W(x,y,z,t) = w(x,y,t) \quad — \end{cases} \quad (2)$$

where *u*, *v* and *w* denote the displacements of the middle plate along the *x*, *y* and *z* axes, respectively. Based on Eq.

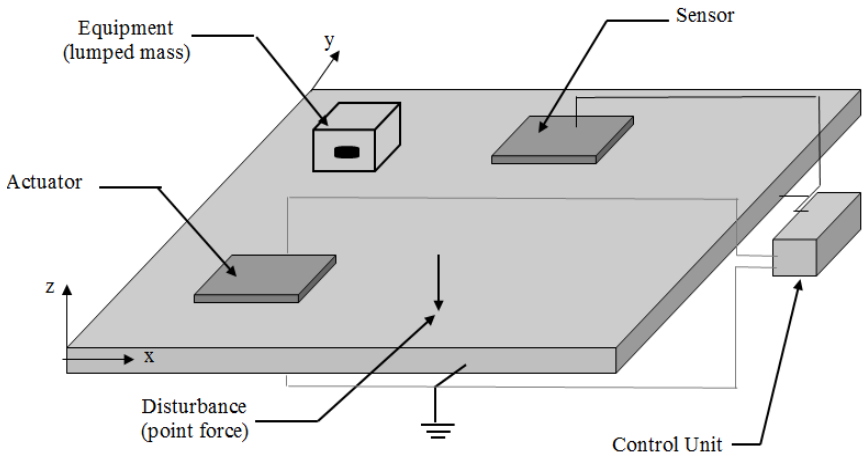

Fig. 2 Model layout of sandwich panel with considering sensor and actuator

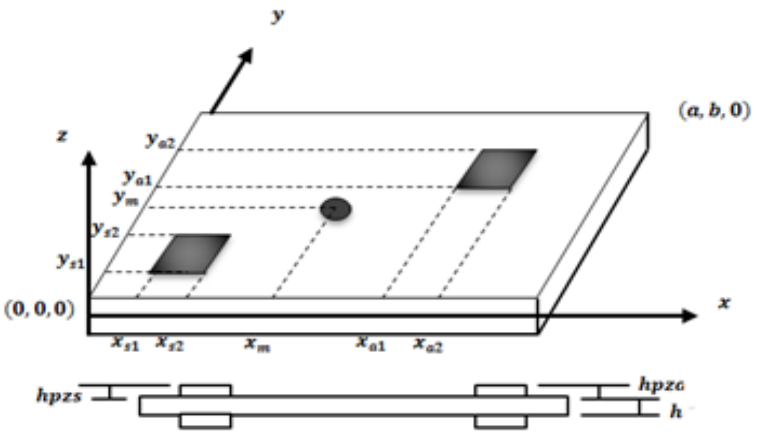

Fig. 3 Plan and side views of sandwich panel as two sensors and actuators

(2), normal and shear strain relations can be obtained as follows

$$\begin{Bmatrix}\varepsilon_{xx}\\ \varepsilon_{xx}\\ \gamma_{xy}\end{Bmatrix}=\begin{Bmatrix}\dfrac{\partial U}{\partial x}\\ \dfrac{\partial \mathrm{V}}{\partial y}\\ \dfrac{\partial U}{\partial x}+\dfrac{\partial \mathrm{V}}{\partial y}\end{Bmatrix}=\begin{Bmatrix}\dfrac{\partial u}{\partial x}\\ \dfrac{\partial v}{\partial y}\\ \dfrac{\partial u}{\partial x}+\dfrac{\partial v}{\partial y}\end{Bmatrix}+z\begin{Bmatrix}-\dfrac{\partial^2 w}{\partial x^2}\\ +\dfrac{\partial^2 w}{\partial y^2}\\ -2\dfrac{\partial^2 w}{\partial x\partial y}\end{Bmatrix} \quad (3)$$

$$\begin{Bmatrix}\gamma_{xz}\\ \gamma_{yz}\end{Bmatrix}=\begin{Bmatrix}0\\ 0\end{Bmatrix}$$

Due to the small displacements, the values of u and v can be ignored. The constitutive equations for the sandwich plate composed of homogenous aluminum honeycomb core and nanocomposite facesheets are written as follows (Mohammadimehr *et al*. 2016a)

$$\begin{Bmatrix}\sigma_{xx}\\ \sigma_{yy}\\ \sigma_{xy}\\ \sigma_{yz}\\ \sigma_{xz}\end{Bmatrix}=\begin{bmatrix}Q_{11} & Q_{12} & 0 & 0 & 0\\ Q_{12} & Q_{22} & 0 & 0 & 0\\ 0 & 0 & Q_{66} & 0 & 0\\ 0 & 0 & 0 & Q_{44} & 0\\ 0 & 0 & 0 & 0 & Q_{55}\end{bmatrix}\begin{Bmatrix}\varepsilon_{xx}\\ \varepsilon_{yy}\\ \gamma_{xy}\\ \gamma_{yz}\\ \gamma_{xz}\end{Bmatrix} \quad (4)$$

$$\varepsilon_{zz}=0 \quad (5)$$

$$\begin{aligned}&Q_{11}=\frac{E_{11}}{1-v_{12}v_{12}}, \quad Q_{12}=\frac{v_{12}E_{11}}{1-v_{12}v_{12}},\\ &Q_{22}=\frac{E_{22}}{1-v_{12}v_{12}}, \quad Q_{66}=G_{12}=\frac{E_{11}}{2(1+v_{12})},\\ &Q_{44}=G_{23}, \quad Q_{55}=G_{13}\end{aligned} \quad (6)$$

In Eq. (6), E_{11}, E_{22}, v_{12}, G_{13}, G_{23}, G_{12} and Q parameters are Young moduli in x and y directions, Poisson's ratio, shear moduli in three directions, and stress constants, respectively.

To simplify the system equations, vibration mode shapes method is applied. The displacement field (out-of-plane displacement w) is described by a superposition of shape functions $s_{m,n}$ (consisting of the first $N=N_m\times N_n$ modes of the bare panel) multiplied by the time-dependent modal coordinates $\Psi_{m,n}$ i.e.

$$w(x,y,t)=\sum_{m=1}^{N_m}\sum_{n=1}^{N_n}s_{m,n}(x,y)\Psi_{m,n}(t)=s^T\Psi \quad (7)$$

where the $N\times 1$ column vectors s and Ψ contain the shape functions and modal coordinates, respectively. The mode shapes of the bare panel

$$s_{m,n}(x,y)=\sin\left(\frac{m\pi x}{a}\right)\sin\left(\frac{n\pi x}{b}\right) \quad (8)$$

are taken as Ritz functions to model the displacement field.

4. Lagrange equations

By the use of Lagrange equations, dynamic equations of the plate can be derived as follows

$$\begin{cases}L=T-U & —\\ \dfrac{d}{dt}\left(\dfrac{\partial L}{\partial \dot{q}_i}\right)-\dfrac{\partial L}{\partial q_i}=Q_i\end{cases} \quad (9)$$

where T and U are the kinetic and potential energies of the system, and $\mathrm{q_i}$ and Qi are the ith generalized coordinate and force, respectively. Of the generalized coordinates are Ψ together with the voltages at the piezoelectric patches.

Q is expressed by point forces acting on the sandwich plate in the coordinate system as follows

$$\begin{cases}Q_i=\sum_{j=1}^{N_f}F_j\dfrac{\partial w_j}{\partial \Psi_j}\\ Q=s_f^T f \quad —\end{cases} \quad (10)$$

where f and S_f column vectors are external forces and modal shape, respectively, at the corresponding force locations. f is the $N_f\times 1$ column vector of forces and S_f, given by Eq. (8), is evaluated at its corresponding force location.

4.1 Kinetic energy

To compute the kinetic energy of the solar panel, the energy of each layer including the core, composite reinforced by carbon nanotube facesheets, piezoelectric layers, and the lumped mass must be calculated in the following form

$$\begin{aligned}T=&T_c+T_{fs_{\mathrm{t}}}+T_{fs_{\mathrm{b}}}+T_{pzs_{\mathrm{t}}}\\ &+T_{pzs_{\mathrm{b}}}+T_{pza_{\mathrm{t}}}+T_{pza_{\mathrm{b}}}+T_{lm}\end{aligned} \quad (11)$$

The general equation to calculate kinetic energy is

$$\begin{aligned}T&=\int\frac{1}{2}\rho\left(\left(\frac{\partial U}{\partial t}\right)^2+\left(\frac{\partial V}{\partial t}\right)^2+\left(\frac{\partial W}{\partial t}\right)^2\right)dV\\ &=\frac{1}{2}\rho\int\left(z^2\left(\frac{\partial s^T}{\partial x}\frac{\partial\Psi}{\partial t}\right)^2+z^2\left(\frac{\partial s^T}{\partial y}\frac{\partial\Psi}{\partial t}\right)^2\right.\\ &\quad\left.+\left(s^T\frac{\partial\Psi}{\partial t}\right)^2\right)dV\\ &=\frac{1}{2}\left(\frac{\partial\Psi}{\partial t}\right)^T\int\rho\left(z^2\frac{\partial s}{\partial x}\frac{\partial s^T}{\partial x}+z^2\frac{\partial s}{\partial y}\frac{\partial s^T}{\partial y}\right.\\ &\quad\left.—+s.s^T\right)dV\left(\frac{\partial\Psi}{\partial t}\right)=\frac{1}{2}\ddot{\Psi}^T M\ddot{\Psi}\end{aligned} \quad (12)$$

where p denotes the material density. The total weight of the plate is obtained from the sum of core, composite reinforced by carbon nanotube facesheets, piezoelectric layers, and the lumped mass weights as shown in appendix A.

$$M_c=\sum_{i=1}^{N_{pz}}\iiint\rho_c\left(z^2\frac{\partial s}{\partial x}\frac{\partial s^T}{\partial x}+z^2\frac{\partial s}{\partial y}\frac{\partial s^T}{\partial y}\right.\\ \left.—+s.s^T\right)dxdy \quad (13)$$

$$M_{fs} = \sum_{i=1}^{N_{pz}} \iiint \rho_{fs} \left(z^2 \frac{\partial s}{\partial x}\frac{\partial s^T}{\partial x} + z^2 \frac{\partial s}{\partial y}\frac{\partial s^T}{\partial y} - + s.s^T \right) dxdy \quad (14)$$

$$M_{pz} = \sum_{i=1}^{N_{pz}} \iiint \rho_{pz} \left(z^2 \frac{\partial s}{\partial x}\frac{\partial s^T}{\partial x} + z^2 \frac{\partial s}{\partial y}\frac{\partial s^T}{\partial y} - + s.s^T \right) dxdy \quad (15)$$

$$M_{lm} = \sum_{i=1}^{N_{pz}} M_{lm_i} s_{lm_i} {s_{lm_i}}^T \quad (16)$$

ρ_c, ρ_{fs} and ρ_{pz_i} are densities of the sandwich core, CNTRC facesheet, piezoelectric patches, respectively. N_1 is the number of lumped masses acting on the sandwich panel. s_{lm_i} denotes the mode shape vector at its corresponding location. The thickness in the top and bottom composite facesheets can be different. N_{pz} represents the number of piezoelectric patches.

4.2 The potential energy

The total potential energy of the sandwich plate is derived from the sum of core, CNTRC facesheets, piezoelectric layers, and the lumped mass potential energies.

$$\begin{aligned} U = U_c + U_{fst} + U_{fsb} \\ + U_{pzs_t} + U_{pzs_b} + U_{pza_t} + U_{pza_b} \end{aligned} \quad (17)$$

To obtain the potential energy stored due to the elasticity of the panel, the following expression is used as seen in appendix B

$$\begin{aligned} \varepsilon^T \sigma &= \begin{bmatrix} \varepsilon_{xx} & \varepsilon_{yy} & \gamma_{xy} & \gamma_{yz} & \gamma_{xz} \end{bmatrix} \begin{bmatrix} \sigma_{xx} \\ \sigma_{yy} \\ \sigma_{xy} \\ \sigma_{yz} \\ \sigma_{xz} \end{bmatrix}^T \\ &= \Psi^T \left(Q_{11} \left(z^2 \frac{\partial^2 s}{\partial x^2}\frac{\partial^2 s^T}{\partial x^2} \right) + Q_{22} \left(z^2 \frac{\partial^2 s}{\partial y^2}\frac{\partial^2 s^T}{\partial y^2} \right) \right. \\ &\left. + 2Q_{12} \left(z^2 \frac{\partial^2 s}{\partial x^2}\frac{\partial^2 s^T}{\partial y^2} \right) + Q_{66} \left(4z^2 \frac{\partial^2 s}{\partial x \partial y}\frac{\partial^2 s^T}{\partial x \partial y} \right) \right) \Psi \end{aligned} \quad (18)$$

For the homogenous core of the sandwich panel, the potential energy is written as follows

$$U_c = \frac{1}{2} \int_0^a \int_0^b \int_{-\frac{h_c}{2}}^{\frac{h_c}{2}} \varepsilon^T \sigma_c \, dxdydz = \frac{1}{2} \Psi^T K_c \Psi \quad (19)$$

$$\begin{aligned} K_c = \int_0^a \int_0^b \int_{-\frac{h_c}{2}}^{\frac{h_c}{2}} \left(Q_{11c} \left(z^2 \frac{\partial^2 s}{\partial x^2}\frac{\partial^2 s^T}{\partial x^2} \right) \right. \\ + Q_{22c} \left(z^2 \frac{\partial^2 s}{\partial y^2}\frac{\partial^2 s^T}{\partial y^2} \right) + 2Q_{12c} \left(z^2 \frac{\partial^2 s}{\partial x^2}\frac{\partial^2 s^T}{\partial y^2} \right) \\ \left. + Q_{66c} \left(4z^2 \frac{\partial^2 s}{\partial x \partial y}\frac{\partial^2 s^T}{\partial x \partial y} \right) \right) dxdydz \end{aligned} \quad (20)$$

For the CNTRC facesheet, the potential energy is obtained from the following expression (appendix C)

$$U_{fs} = \frac{1}{2} \iiint \varepsilon^T \sigma_{fs} \, dxdydz = \frac{1}{2} \Psi^T K_{fs} \Psi \quad (21)$$

$$\begin{aligned} K_{fs} = \iiint \left(Q_{11f} \left(z^2 \frac{\partial^2 s}{\partial x^2}\frac{\partial^2 s^T}{\partial x^2} \right) \right. \\ + Q_{22f} \left(z^2 \frac{\partial^2 s}{\partial y^2}\frac{\partial^2 s^T}{\partial y^2} \right) + 2Q_{12f} \left(z^2 \frac{\partial^2 s}{\partial x^2}\frac{\partial^2 s^T}{\partial y^2} \right) \\ \left. + Q_{66f} \left(4z^2 \frac{\partial^2 s}{\partial x \partial y}\frac{\partial^2 s^T}{\partial x \partial y} \right) \right) \end{aligned} \quad (22)$$

For the piezoelectric patches, the potential energy includes three energy components, i.e., the energy stored due to the elasticity of the material, the additional energy due to voltage-driven piezoelectric effect, and the electric energy stored due to the dielectric characteristics of the piezoelectric material. Therefore, the potential energy can be written as

$$U_{pz} = U_{pz_{\text{elast}}} + U_{pz_{\text{elastelect}}} + U_{pz_{\text{elect}}} \quad (23)$$

When calculating the potential energy stored due to the elastic energy of piezoelectric patches, the following assumptions must be taken into account (Aglietti *et al.* 2004):

(i) The stiffness of the electrodes attached to the piezoelectric patches is negligible.
(ii) The layer of adhesive connecting the electrodes to the piezoelectric patches has negligible thickness when compared to that of the patches. The adhesive can transfer all of the shear strain.
(iii) No natural boundary conditions at the edges of each patch (i.e., a = 0) exist and do not affect stress/strain distribution through the whole sandwich panel.

The potential energy stored due to the elasticity and isotropy of piezoelectric patches is the same as that of the core and CNTRC facesheets. However, the longitudinal and transverse moduli of elasticity moduli are assumed the same in piezoelectric patches. E_{pzi} denotes the Young's modulus for the ith patch and υ_{pzi} represents Poisson's ratio.

$$\begin{aligned} U_{pz_{\text{elast}}} &= \frac{1}{2} \sum_{i=1}^{N_{pz}} \iiint \varepsilon^T \sigma_{pzi} \, dxdydz \\ &= \frac{1}{2} \Psi^T K_{pz_{\text{elast}}} \Psi \end{aligned} \quad (24)$$

$$K_{pz_{\text{elast}}} = \sum_{i=1}^{N_{pz}} \iiint \frac{E_{pz_i} z^2}{(1 - \upsilon_{pzi}^2)} \left[\frac{\partial^2 s_{pzi}}{\partial x^2}\frac{\partial^2 s_{pzi}^T}{\partial x^2} \right. \quad (25)$$

$$+\frac{\partial^2 s_{pzi}}{\partial y^2}\frac{\partial^2 s_{pzi}^T}{\partial y^2}+2\upsilon_{pzi}\frac{\partial^2 s_{pzi}}{\partial x^2}\frac{\partial^2 s_{pzi}^T}{\partial y^2} +2(1-\upsilon_{pzi})\frac{\partial^2 s_{pzi}}{\partial x\partial y}\frac{\partial^2 s_{pzi}^T}{\partial x\partial y}\Bigg] dxdydz \quad (25)$$

In the present study, $N_{pzi}=4$ (two patches of sensor, two patches of actuators in the top and bottom of the sandwich panel). Due to the different direction of strain in the top and bottom of the sandwich panel and also piezoelectric patches being of the same type and size, $K_{pz_{\text{elast}}}$ (the stiff matrix) is the same in the top and bottom of the sandwich panel.

The patch here is assumed to have a constant thickness h_{pz} which is thin enough to prevent fringe effects. It has a voltage v which is applied at its electrodes. Supposing a constant electric field $e=\frac{V_{pz}}{h_{pz}}$ across the h_{pz} patch, the further stress resulted from the applied voltages is calculated as

$$\sigma_{\text{elect}}=\begin{pmatrix}\sigma_{x_{\text{elect}}}\\ \sigma_{y_{\text{elect}}}\end{pmatrix}=\frac{E_{pz}}{1-\nu^2}\begin{pmatrix}\epsilon_{xz}+\upsilon\epsilon_{yz}\\ \epsilon_{yz}+\upsilon\epsilon_{xz}\end{pmatrix}e \quad (26)$$

h_{pz} is the thickness of the piezoelectric layer and ϵ_{xz} and ϵ_{pz} are the piezoelectric constants of the material. E_{pz} is Young's modulus constant of the piezoelectric material. Therefore, by assuming that $\epsilon_{xz}=\epsilon_{yz}=\epsilon_z$ and substituting σ_{elect} from Eq. (26) into Eq. (27).

The elastoelectric energy stored in the N_{pz} patches can be written as (Aglietti *et al*. 2000)

$$\begin{aligned}U_{pz_{\text{elastelect}}} &=\frac{1}{2}\sum_{i=1}^{N_{pz}}\iiint \varepsilon^T\sigma_{\text{elect}}\ dxdydz\\ &=\frac{1}{2}\sum_{i=1}^{N_{pz}}\iiint \left(\varepsilon_{xx}\sigma_{x_{\text{elect}}}+\varepsilon_{yy}\sigma_{y_{\text{elect}}}\right) dxdydz\\ &=\frac{1}{2}\sum_{i=1}^{N_{pz}}\iiint \left(z\frac{\partial^2 s_{pzi}^T\Psi}{\partial x^2}+z\frac{\partial^2 s_{pzi}^T\Psi}{\partial y^2}\right) \frac{E_{pz_i}\epsilon_{z_i}e_i}{(1-\nu_{pz_i})}dxdydz\\ &=V_{pz}^T K_{pz_{\text{elastelect}}}\ \Psi\end{aligned} \quad (27)$$

Considering the symmetry in $\varepsilon^T\sigma_{\text{elect}}=\sigma_{\text{elect}}{}^T\varepsilon$, Eq. (27) is derived in the following form

$$K_{pz_{\text{elastelect}}}^T =\sum_{i=1}^{N_{pz}}\iiint \frac{E_{pz_i}\epsilon_{z_i}p_i}{2(1-\nu_{pz_i})}\left(z\frac{\partial^2 s_{pzi}^T}{\partial x^2}+z\frac{\partial^2 s_{pzi}^T}{\partial y^2}\right)dxdydz \quad (28)$$

In Eq. (28), $p_i=\frac{1}{h_{pz_i}}$. Since the potential energy function is even, it would be equal for the piezoelectric patches in the top and bottom of the sandwich panel.

The potential energy due to the electric field is obtained from $d_i=\epsilon_{pz_i}\frac{V_{pz}}{h_{pz_i}}$. d is the electric displacement and ϵ_{pz_i} is the dielectric constant of the piezoelectric material.

$$\begin{aligned}U_{pz_{\text{elect}}} &=\frac{1}{2}\sum_{i=1}^{N_{pz}}\iiint e^T d\ dxdydz\\ &=\frac{1}{2}\sum_{i=1}^{N_{pz}}\iiint \left(\frac{V_{pz}}{h_{pz_i}}\right)^T\epsilon_{pz_i}\frac{V_{pz}}{h_{pz_i}}\ dxdydz\\ &=\frac{1}{2}V^T K_{pz_{\text{elect}}}\ V\end{aligned} \quad (29)$$

$$K_{pz_{\text{elect}}}=\frac{1}{2}\sum_{i=1}^{N_{pz}}\iiint \epsilon_{pz_i}P_i^T P_i\ dxdydz \quad (30)$$

Due to the symmetric distribution of the electric energy in the top and bottom of the sandwich panel in piezoelectric patches, $U_{pzt_{\text{elect}}}=U_{pzb_{\text{elect}}}$. Therefore, the general relation for the potential energy is

$$U=\frac{1}{2}\Psi^T K_c\ \Psi+\frac{1}{2}\Psi^T K_{fs}\ \Psi+\frac{1}{2}\Psi^T K_{pz_{\text{elect}}}\ \Psi +V_{pz}^T K_{pz_{\text{elastelect}}}\ \Psi+\frac{1}{2}V_{pz}^T K_{pz_{\text{elect}}}\ V_{pz} \quad (31)$$

Substituting the kinetic and potential energies and the generalized forces from Eqs. (12)-(31) and (10) into Eq. (9) and derivation of Ψ and V_{pz} yields the following equations

$$\left(M_c+M_{fs}+M_{pz}+M_{lm}\right)\ddot{\Psi} +\left(K_c+K_{fs}+K_{pz_{\text{elect}}}\right)\Psi+K_{pz_{\text{elastelect}}}^T\ V_{pz}=s_f^T F \quad (32)$$

$$K_{pz_{\text{elastelect}}}\ \Psi+K_{pz_{\text{elect}}}\ V_{pz}=0 \quad (33)$$

Using

$$M=M_c+M_{fs}+M_{pz}+M_{lm} \quad (34)$$

$$K_{\text{elast}}=K_c+K_{fs}+K_{pz_{\text{elect}}} \quad (35)$$

$$K_{pz_{\text{elastelect}}}^T\ V_{pz}=\begin{bmatrix}K_{pzs_{\text{elastelect}}}^T & K_{pza_{\text{elastelect}}}^T\end{bmatrix}\begin{bmatrix}V_{pzs}\\ V_{pza}\end{bmatrix} \quad (36)$$

Eq. (32) can be written as follows

$$M\ddot{\Psi}+K_{\text{elast}}\Psi+K_{pzs_{\text{elastelect}}}^T\ V_{pzs} +K_{pza_{\text{elastelect}}}^T\ V_{pza}=s_f^T F \quad (37)$$

Based on Eq. (33), the piezoelectric voltage obtained from measuring the sensor is

$$V_{pzs}=-K_{pzs_{\text{elect}}}{}^{-1}K_{pzs_{\text{elastelect}}}\ \Psi \quad (38)$$

Substituting Eq. (38) into Eq. (37) yields the following equation

$$M\ddot{\Psi}+\left(K_{\text{elast}}-K_{pzs_{\text{elastelect}}}^T\ K_{pzs_{\text{elect}}}{}^{-1}K_{pzs_{\text{elastelect}}}\right)\Psi =-K_{pza_{\text{elastelect}}}^T\ V_{pza}+s_f^T F \quad (39)$$

Considering $K_{pzs} = K_{pzs}^{T}{}_{\text{elastelect}}\ K_{pzs}{}_{\text{elect}}{}^{-1} K_{pzs}{}_{\text{elastelect}}$, Eq. (39) is simplified as follows

$$M\ddot{\Psi} + \left(K_{\text{elast}} + K_{pzs}\right)\Psi = -K_{pza}^{T}{}_{\text{elastelect}}\ V_{pza} + s_f^T F \quad (40)$$

Adding damping matrix and defining $K = K_{\text{elast}} + K_{pzs}$ for Eq. (40) yields the following equations for solar panels with honeycomb core and carbon nanotube reinforced composite facesheets

$$M\ddot{\Psi} + C_s\dot{\Psi} + K\Psi = -K_{pza}^{T}{}_{\text{elastelect}}\ V_{pza} + s_f^T F \quad (41)$$

where [M], [K], [F], [V_{pza}] are the global mass matrix, the global stiffness matrix, the external force vector, and the control force vector, respectively. [C_s] = α[M]+β[K] is the damping matrix of which α and β are the constants (Qiu and Ling 2014).

5. Control system

The mathematical model obtained from Eqs. (7)-(38) and (41) in state-space form can be written as

$$w_{\text{out}} = C_w x \quad (42)$$

$$v_s = C_v x \quad (43)$$

$$\dot{x} = Ax + B_v v_a + B_f f \quad (44)$$

where

$$x = \begin{pmatrix} x_1 \\ x_2 \end{pmatrix} = \begin{pmatrix} \Psi \\ \dot{\Psi} \end{pmatrix}, \quad \begin{cases} \dot{x}_1 = x_2 \\ \dot{x}_2 = -M^{-1}Kx_1 - M^{-1}C_s x_2 - M^{-1} K_{pza}^{T}{}_{\text{elastelect}}\ V_{pza} + M^{-1}s_f^T F \end{cases} \quad (45)$$

Therefore

$$A = \begin{bmatrix} 0 & 1 \\ -M^{-1}K & -M^{-1}C_s \end{bmatrix}, \quad B_v = \begin{bmatrix} 0 \\ -M^{-1}K_{pza}^{T}{}_{\text{elastelect}} \end{bmatrix}, \quad B_f = \begin{bmatrix} 0 \\ M^{-1}s_f^T \end{bmatrix} \quad (46)$$

$$C_v = \left[-K_{pzs}{}_{\text{elect}}{}^{-1}K_{pzs}{}_{\text{elastelect}} \quad 0\right], \quad C_w = [s_{\text{out}}^T \quad 0] \quad (47)$$

where K denotes the total stiffness matrix, w_{out} is the output displacement of the sandwich panel specified by s_{out}, the vibration mode shape vectors. By the use of the obtained relations in state-space form and their linearity, state feedback design based on linear quadratic regulator (LQR) can be of the optimal approaches for the controller which mainly focuses on minimizing the following cost function (Murray 2006)

$$J = \int_0^{\infty} (w_{\text{out}}^T Q w_{\text{out}} + v_a^T R v_a) dt \quad (48)$$

where the symmetric weighting matrices Q and R are positive semi-definite and positive definite, respectively. They are of the same dimensions with system state variables and selecting them depends on the controller's designer. Based on state feedback law

$$V_{pza} = G_{fs} x \quad (49)$$

where G_{fs} is the state-feedback matrix and generated as follows

$$G_{fs} = R^{-1} B v^T P_c \quad (50)$$

And P_c in Eq. (50) is satisfied in the algebraic Riccati equation as follows

$$A^T P_c + P_c A - P_c B_v R^{-1} B_v^T P_c + C_w Q C_w^T = 0 \quad (51)$$

Table 1 Mechanical properties of materials for sandwich panels

	Material dimensions	Material properties
Aluminum plate	$a = 304.8mm$ $b = 203.2mm$ $h = 21mm$	$E1 = 72\ GPa\ ,\ E2 = 72\ GPa$ $G12 = 27\ GPa$ $\rho = 2700\ kgm^{-3}, \upsilon = 0.33$
CNTRC facesheet	$a = 304.8mm$ $b = 203.2mm$ $h = 0.5mm$	$E1 = 5.64\ TPa\ ,\ E2 = 7.08\ TPa$ $G12 = 1.94\ TPa$,V_{CNT}=0.17, η_1=0.142,η_2=1.626,η_3=1.138 $\rho = 4000\ kgm^{-3}, \upsilon = 0.175$
Aluminum core 5052	$a = 304.8mm$ $b = 203.2mm$ $h = 20mm$	$E1 = 0.41\ GPa\ ,\ E2 = 0.24\ GPa$ $G12 = 0.22\ GPa$ $\rho = 37\ kgm^{-3}, \upsilon = 0.33$
sensor	$xs1 = 0.8mm\ ,\ xs2 = 101.6mm$ $ys1 = 25.4mm\ ,\ ys2 = 76.2mm$ $hpzs = 0.19mm$	$E = 63e9\ Pa$ $\rho = 7650\ kgm^{-3},\ \upsilon = 0.3$ $D = 1.66e-10\ mv^{-1}\ ,\ \varepsilon = 1700\ \varepsilon^0$
Actuator	$xa1 = 76.2mm\ ,\ xa2 = 127mm$ $ya1 = 101.6mm\ ,\ ya2 = 152.4mm$ $hpza = 0.19mm$	$E = 63e9\ Pa$ $\rho = 7650\ kgm^{-3},\ \upsilon = 0.3$ $D = 1.66e-10\ mv^{-1}\ ,\ \varepsilon = 1700\ \varepsilon^0$
Lumped mass	$Xlm = 50.8mm\ ,\ Ylm = 152.4mm$	$Wlm = 50g$

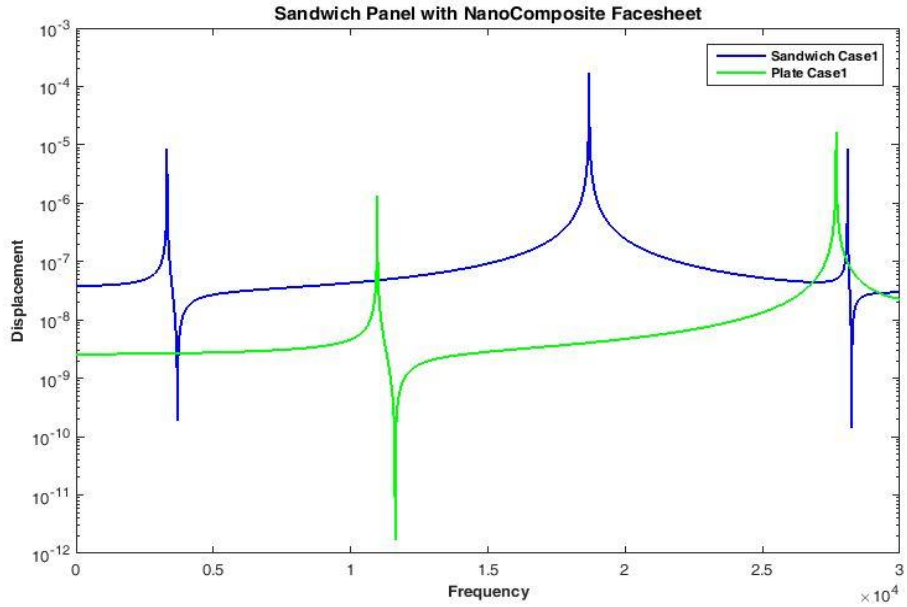

Fig. 4 Comparison of the sandwich panel and aluminum plate in test case 1

6. Results and simulation

We have come across different interpretations of analytical vs. numerical methods in books and articles. One of the explanations suggests that analytical methods give exact solutions while numerical methods give approximate solutions. If we follow this definition, methods like the Adomian decomposition, homotopy analysis & perturbation, Taylor series expansion, and even Picard's. In fact, in this case almost all methods - except very few ones - are numerical. Another explanation suggests that the difference is that an analytical method gives a solution in the form of symbols i.e., closed form solution. On the other hand, a numerical method gives solutions at certain points only. If we follow this explanation, the aforementioned methods will be all analytical since they produce closed form solutions. In this case, methods like the finite difference and finite element are numerical since they give results at certain points.

Given the system has two inputs, i.e., Force and Actuator voltage, the results and simulation were analyzed considering two test cases:

Test case 1: the disturbance consists of a harmonic point force of amplitude 1 N perpendicular to the panel at a specific location x = 254 mm and y = 50.8 mm, which is written as follows

$$f = Fe^{jwt} \tag{52}$$

And also a lumped mass weighing 50 g is applied at x = 50.8 mm and y = 154.2 mm.

Test case 2: Sinusoidal voltage of 1 volt is applied into the piezoelectric actuator. Voltage function is in the following form

Table 2 Comparison of the sandwich panel and aluminum plate in the first three frequencies and displacements in test state 1

	Frequency 1	Frequency 2	Frequency 3	Displacement 1	Displacement 2	Displacement 3
Sandwich panel (present)	3320	3700	18690	8.41e-6	2.56e-10	1.03e-4
Aluminum plate (Kumar and Narayanan 2008)	10980	11630	27690	5.12e-7	1.69e-12	1.62e-5

Table 3 Comparison of the sandwich panel and aluminum plate in the first three frequencies and displacements in test state 2

	Frequency 1	Frequency 2	Frequency 3	Displacement 1	Displacement 2	Displacement 3
Sandwich panel (present)	161© 50	24470	26560	3.24e-5	5.97e-9	2.81e-6
Aluminum plate (Kumar and Narayanan 2008)	27530	27660	27700	4.97e-6	9.12e-9	2.98e-6

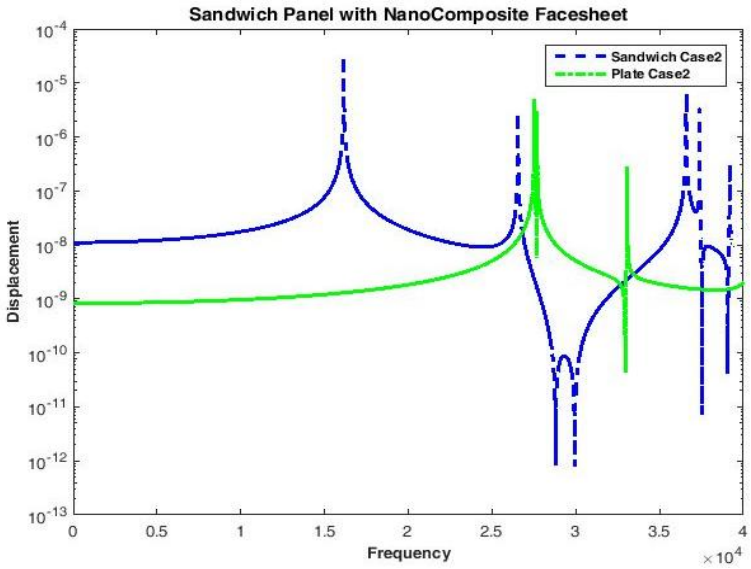

Fig. 5 Comparison of the sandwich panel and aluminum plate in test case 2

$$V_{pza} = Ve^{jwt} \tag{53}$$

To simulate the equations of the system, up to 36 mode shape vectors were considered so that the stress strain behavior of the panel and extent of displacement would be thoroughly evaluated.

$$w = s^T\Psi = (s_1 \dots s_{36})(\Psi_1 \dots \Psi_{36})^T \tag{54}$$

The properties of the sandwich panel, piezoelectric patches, CNTRC facesheets, and the honeycomb core are given in Table 1 (Aglietti *et al*. 1997, Kim and Lee 2008).

The displacements of an aluminum plate and a sandwich panel in the frequency domain of 30 kHz in test case 1 are shown in Fig. 4. Material properties of the CNTRC facesheet are given as

$$E_m^c = 8.3 \text{ GPa}, \quad v_m^c = 0.18, \quad \rho_m^c = 1750 \text{ Kgm}^{-3}$$

As seen in Fig. 4, the displacement of the sandwich panel being close to that of aluminum plate is indicative of the high robustness of the sandwich panel the core density of which is 73 times as small as the aluminum plate. The reason for the robustness is the use of carbon nanotube reinforced composite in the structure of the sandwich panel facesheets which is verified by the value of Young's modulus of nanotube particles in Table 1. The displacements of the sandwich panel and the aluminum plate in the first three frequency mode for test cases 1 and 2 are shown in Tables 2-3.

In Fig. 5, the same comparison is made between the sandwich panel and aluminum plate. However, in contrast to the test case 1 in which inputs are the disturbance force and a lumped mass applied, here the only input is the piezoelectric actuators voltage.

Although the sandwich panel has vibrations close to that of the aluminum plate in Fig. 4, the extremums are more compared to those in. The reason is that the disturbance force would be smaller than the piezoelectric actuator voltage as their coefficients are different.

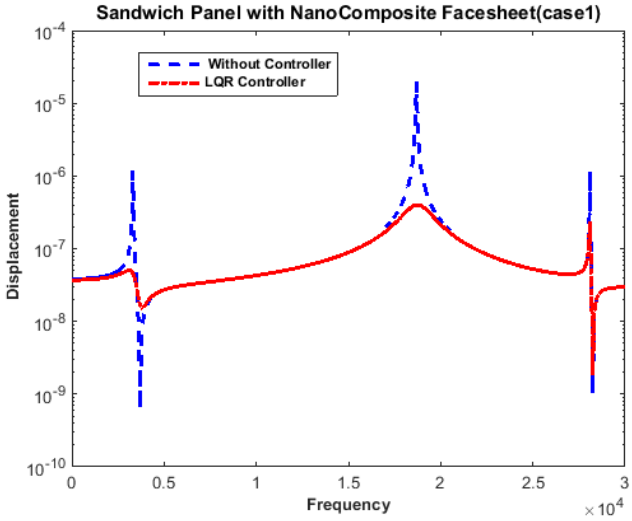

Fig. 6 Frequency response of the sandwich panel with LQR controller

In Fig. 6, linear quadratic regulator (LQR) is used to decrease the vibrations of the sandwich panel. Controller coefficients have been selected as $R = 1$ and $Q = 10^{13}$ to yield the best performance of the controller and the least vibrations of the panel. The reason for the large difference between R and Q in the controller is the large difference between the mass and the stiffness matrices in the sandwich panel. Eigenvalues of mass matrix are about 10^{-3} when eigenvalue of stiffness matrix are about 10^{12}.

Since the system matrix has its own eigenvalues on the left side of the imaginary axis, it can be said that it has inner stability. For better understanding, Figs. 7-9 present the effect of uncertainties on the performance of the system in the force position (tolerance = 6 mm), the lumped mass position (tolerance = 3 mm)and lumped mass weight (tolerance = 3 gr). Differences are shown in larger scales,

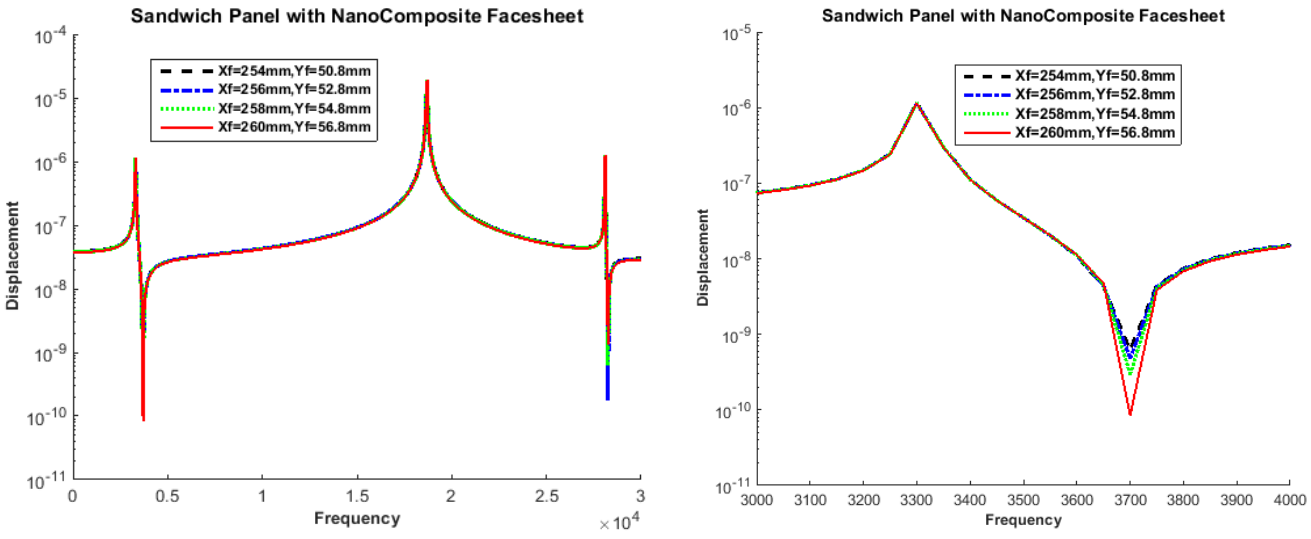

(a) (b)

Fig. 7 (a) Stability to uncertainty in the force position; (b) Stability to uncertainty in the force position (First and Second Natural Frequency)

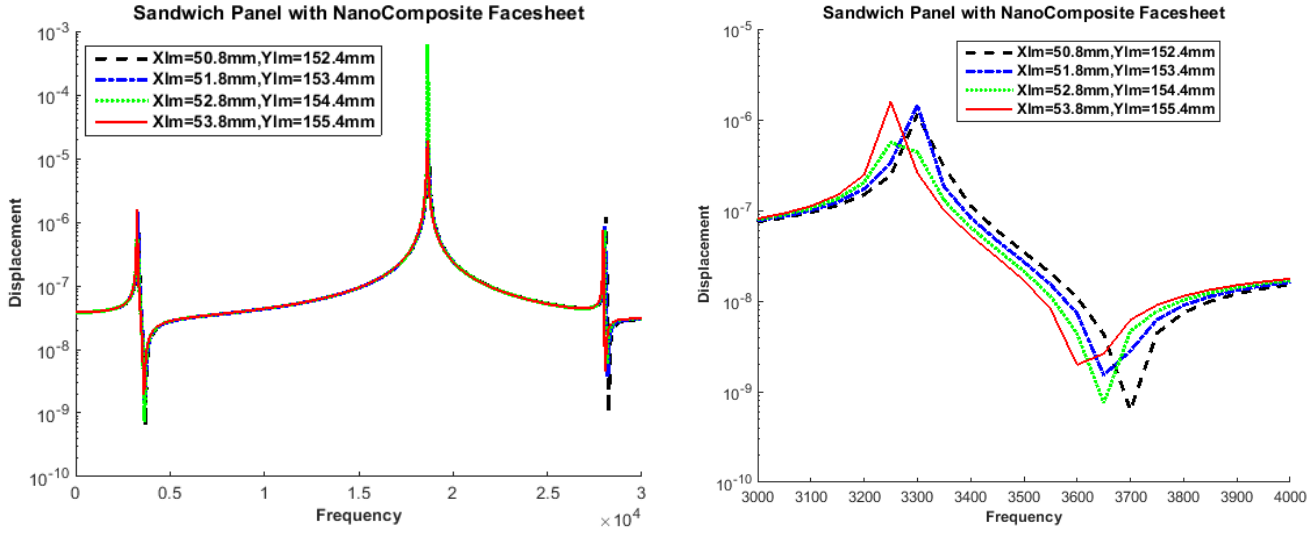

(a) (b)

Fig. 8 (a) Stability to uncertainty in the lumped mass position; (b) Stability to uncertainty in the lumped mass position (First and Second Natural Frequency)

i.e., between 3000 to 4000 Hz.

Variations in core-to-facesheet thickness ratio are very important in the robustness of a sandwich panel. The increase in the ratio of the core thickness to that of the nanocomposite facesheet would decrease the robustness of the sandwich panel (Fig. 10). These variations are shown numerically in Table 4.

Another important factor in the optimization of the control parameters of the system is positioning the piezoelectric patches. Robustness to changing the position between the sensor and the actuator on the top facesheet can be seen in Fig. 11. Differences have been shown in larger scales, i.e., between 3000 to 4000 Hz.

7. Conclusions

In the present study, with the application of the dynamic equations of a sandwich panel based on Lagrange equations and presentation of a very precise model of piezoelectric patches properties and performance, a linear, simple and efficient equation was obtained. By the use of the first 36 mode shape a vector, an accurate model of dynamic system was obtained that can be evaluated with the finite element method. Performance analysis of a sandwich panel with the honeycomb core and carbon nanotube reinforced composite facesheets revealed its inner stability against uncertainties. Due to the presence of system eigenvalues on the left side

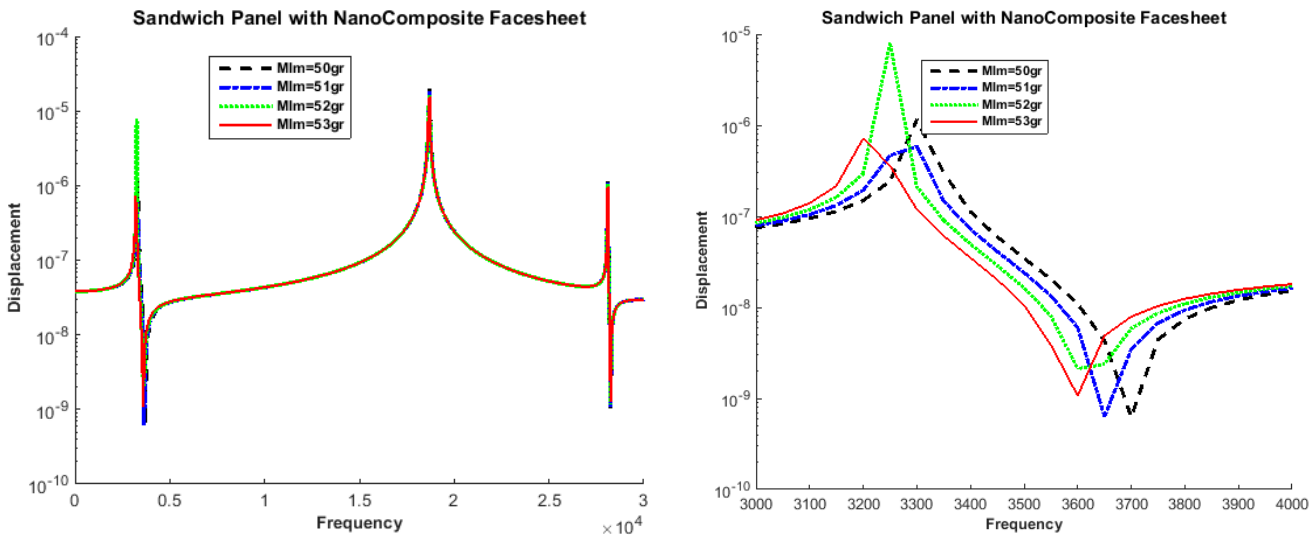

(a) (b)

Fig. 9 (a) Stability to uncertainty in the lumped mass weight; (b) Stability to uncertainty in the lumped mass weight (First and Second Natural Frequency)

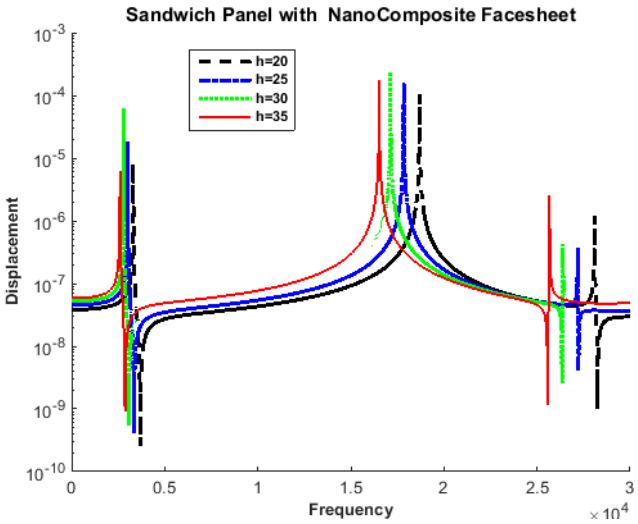

Fig. 10 Reduction of robustness with the increase in core-to-facesheet thickness ratio

of the imaginary axis, using a model-based the second order linear regression controller was the best option. As proved in the study, the utilization of the sandwich panel in the structure and skeleton of the satellites caused the decrease in weight and no change in its robustness. As a matter of fact, given the effects of different parameters such as weight and the position of the lumped mass, core to facesheet thickness ratio, and the position of the piezoelectric patches, robustness properties in the sandwich panel were revealed. Last but not least, Solar radiation and aerodynamic forces are about 10^{-4} N.m. This number is far smaller compared to the disturbance force in this article, which is about 1 N.m. Thus, with the help of LQR controller, vibration suppression can occur in the sandwich panel.

Acknowledgments

The authors would like to thank the referees for their valuable comments. Also, they are thankful to the Iranian Nanotechnology Development Committee for their financial support and the University of Kashan for supporting this work by Grant No. 682561/21.

References

Aglietti, G.S., Gabriel, S.B., Langley, R.S. and Rogers, E. (1997), "A modeling technique for active control design studies with application to spacecraft microvibrations", *J. Acoust. Soc. Am.*, **102**(4), 2158-2166. https://doi.org/10.1121/1.419631

Table 4 Comparison of displacements and frequencies with the increase in core-to-facesheet thickness ratio

Thickness (h_c/h_{fs})	Frequency 1	Frequency 2	Frequency 3	Displacement 1	Displacement 2	Displacement 3
h = 20	3320	3700	18690	8.41e-6	2.56e-10	1.03e-4
h = 25	3020	3360	17850	1.82e-5	4.07e-10	1.62e-4
h = 30	2790	3090	17140	6.13e-5	5.48e-10	2.28e-4
h = 35	2610	2880	16530	6.99e-5	9.12e-10	2.76e-4

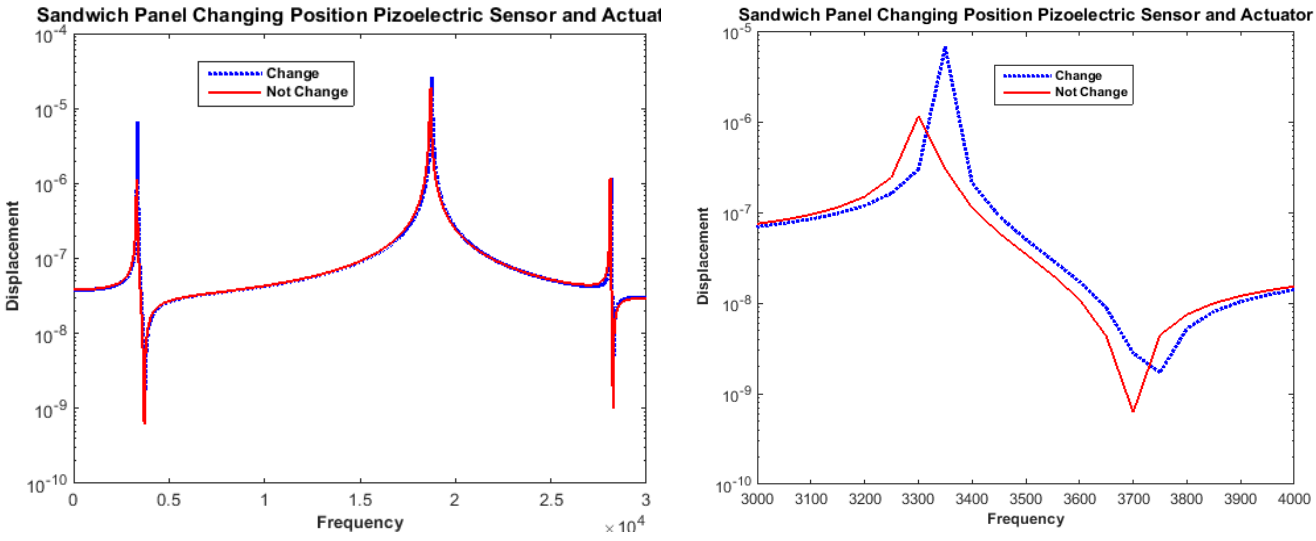

(a) (b)

Fig. 11 (a) Reduction of robustness with the change of position between sensor and actuator; (b) Reduction of robustness with the change of position between sensor and actuator(First and Second Natural Frequency)

Aglietti, G.S., Langley, R.S., Rogers, E. and Gabriel, S.B. (2000), "An efficient model of an equipment loaded panel for active control design studies", *J. Acoust. Soc. Am.*, **108**(4), 1663-1673. https://doi.org/10.1121/1.1287844

Aglietti, G.S., Stoustrup, J., Langley, R.S., Rogers, E. and Gabriel, S.B. (2002), "Modelling and feedback control of micro-vibrations", In: *The Institution of Electrical Engineers*, pp. 241-274.

Aglietti, G.S., Langley, R.S., Rogers, E. and Gabriel, S.B. (2004), "Model building and verification for active control of microvibrations with probabilistic assessment of the effects of uncertainties", *Proceedings of the Institution of Mechanical Engineers, Part C: J. Mech. Eng. Sci.*, **218**(4), 389-399. https://doi.org/10.1177/095440620421800404

Arani, A.G. and Kiani, F. (2018), "Nonlinear free and forced vibration analysis of microbeams resting on the nonlinear orthotropic visco-Pasternak foundation with different boundary conditions", *Steel Compos. Struct., Int. J.*, **28**(2), 149-165. https://doi.org/10.12989/scs.2018.28.2.149

Arani, A.G., Hashemian, M., Loghman, A. and Mohammadimehr, M. (2011), "Study of dynamic stability of the double-walled carbon nanotube under axial loading embedded in an elastic medium by the energy method", *J. Appl. Mech. Tech. Phys.*, **52**(5), 815-824. https://doi.org/10.1134/S0021894411050178

Aydin, M.R. and Gundogdu, O. (2018), "Vibration analysis of honeycomb sandwich composites filled with polyurethane foam by Taguchi Method", *Steel Compos. Struct., Int. J.*, **28**(4), 461-470. https://doi.org/10.12989/scs.2018.28.4.461

Bui, T.Q., Khosravifard, A., Zhang, C., Hematiyan, M.R. and Golub, M.V. (2013), "Dynamic analysis of sandwich beams with functionally graded core using a truly meshfree radial point interpolation method", *Eng. Struct.*, **47**, 90-104. https://doi.org/10.1016/j.engstruct.2012.03.041

Chhabra, D., Chandna, P. and Bhushan, G. (2011), "Design and analysis of smart structures for active vibration control using piezo-crystals", *Int. J. Eng. Technol.*, **1**(3), 153-163.

Daouadji, T.H., Benferhat, R. and Adim, B. (2016), "A novel higher order shear deformation theory based on the neutral surface concept of FGM plate under transverse load", *Adv. Mater. Res., Int. J.*, **5**(2), 107-120. https://doi.org/10.12989/amr.2016.5.2.107

Daraji, A.H., Hale, J.M. and Ye, J. (2017), "New methodology for optimal placement of piezoelectric sensor/actuator pairs for active vibration control of flexible structures", *J. Vib. Acoust.*, **140**(1), 011015. https://doi.org/10.1115/1.4037510

Do, T.V., Bui, T.Q., Yu, T.T., Pham, D.T. and Nguyen, C.T. (2017), "Role of material combination and new results of mechanical behavior for FG sandwich plates in thermal environment", *J. Computat. Sci.*, **21**, 164-181. https://doi.org/10.1016/j.jocs.2017.06.015

Emdadi, M., Mohammadimehr, M. and Navi, B.R. (2019), "Free vibration of an annular sandwich plate with CNTRC facesheets and FG porous cores using Ritz method", *Adv. Nano Res., Int. J.*, **7**(2), 109-123. https://doi.org/10.12989/anr.2019.7.2.109

Fang, Y., Fei, J. and Hu, T. (2018), "Adaptive backstepping fuzzy sliding mode vibration control of flexible structure", *J. Low Frequency Noise Vib. Active Control*, **37**(4), 1079-1096. https://doi.org/10.1016/j.jocs.2017.06.015

Han, Y. and Elliott, J. (2007), "Molecular dynamics simulations of the elastic properties of polymer/carbon nanotube composites", *Computat. Mater. Sci.*, **39**(2), 315-323. https://doi.org/10.1016/j.commatsci.2006.06.011

He, X., He, W., Chen, Y., Mu, X., Yu, Y. and Sun, C. (2018), "Boundary control of flexible aircraft wings for vibration suppression", *Int. J. Control*, **10**, 1-10. https://doi.org/10.1080/00207179.2018.1442025

Kim, B.J. and Lee, D.G. (2008), "Characteristics of joining inserts for composite sandwich panels", *Compos. Struct.*, **86**(1), 55-60. https://doi.org/10.1016/j.compstruct.2008.03.020

Kumar, K.R. and Narayanan, S. (2008), "Active vibration control of beams with optimal placement of piezoelectric sensor/actuator pairs", *Smart Mater. Struct.*, **17**(5), 055008. https://doi.org/10.1088/0964-1726/17/5/055008

Kumar, R., Dey, T. and Panda, S.K. (2019), "Instability and vibration analyses of FG cylindrical panels under parabolic axial compressions", *Steel Compos. Struct., Int. J.*, **31**(2), 187-199. https://doi.org/10.12989/scs.2019.31.2.187

Lin, H. and Cao, D.Q. (2018), "A unified Gram-Schmidt-Ritz formulation for vibration and active flutter control analysis of honeycomb sandwich plate with general elastic support", *J. Vibroeng.*, **20**(5), 1982-2000. https://doi.org/10.1088/0964-1726/17/5/055008

Malekzadeh, M., Naghash, A. and Talebi, H.A. (2012), "Robust attitude and vibration control of a nonlinear flexible spacecraft",

Asian J. Control, **14**(2), 553-563. https://doi.org/10.1002/asjc.332

Marynowski, K. (2012), "Dynamic analysis of an axially moving sandwich beam with viscoelastic core", *Compos. Struct.*, **94**(9), 2931-2936. https://doi.org/10.1016/j.compstruct.2012.03.040

Mohammadimehr, M. and Mehrabi, M. (2017), "Stability and free vibration analyses of double-bonded micro composite sandwich cylindrical shells conveying fluid flow", *Appl. Math. Model.*, **47**, 685-709. https://doi.org/10.1016/j.apm.2017.03.054

Mohammadimehr, M. and Rahmati, A.H. (2013), "Small scale effect on electro-thermo-mechanical vibration analysis of single-walled boron nitride nanorods under electric excitation", *Turkish J. Eng. Environ. Sci.*, **37**(1), 1-15.

Mohammadimehr, M. and Shahedi, S. (2017), "High-order buckling and free vibration analysis of two types sandwich beam including AL or PVC-foam flexible core and CNTs reinforced nanocomposite face sheets using GDQM", *Compos. Part B: Eng.*, **108**, 91-107. https://doi.org/10.1016/j.compositesb.2016.09.040

Mohammadimehr, M., Navi, B.R. and Arani, A.G. (2016a), "Dynamic stability of MSGT sinusoidal viscoelastic piezoelectric polymeric FG-SWNT reinforced nanocomposite plate considering surface stress and agglomeration effects under hydro-thermo-electro-magneto-mechanical loadings", *Mech. Adv. Mater. Struct.*, **24**(16), 1325-1342. http://dx.doi.org/10.1080/15376494.2016.1227507

Mohammadimehr, M., Rostami, R. and Arefi, M. (2016b), "Electro-elastic analysis of a sandwich thick plate considering FG core and composite piezoelectric layers on Pasternak foundation using TSDT", *Steel Compos. Struct., Int. J.*, **20**(3), 513-543. https://doi.org/10.12989/scs.2016.20.3.513

Mohammadimehr, M., Zarei, H.B., Parakandeh, A. and Arani, A.G. (2017a), "Vibration analysis of double-bonded sandwich microplates with nanocomposite facesheets reinforced by symmetric and un-symmetric distributions of nanotubes under multi physical fields", *Struct. Eng. Mech., Int. J.*, **64**(3), 361-379. https://doi.org/10.12989/sem.2017.64.3.361

Mohammadimehr, M., Monajemi, A.A. and Afshari, H. (2017b), "Free and forced vibration analysis of viscoelastic damped FG-CNT reinforced micro composite beams", *Microsyst. Technol.*, 1-15. https://doi.org/10.1007/s00542-017-3682-4

Mohammadimehr, M., Shahedi, S. and Rousta Navi, B. (2017c), "Nonlinear vibration analysis of FG-CNTRC sandwich Timoshenko beam based on modified couple stress theory subjected to longitudinal magnetic field using generalized differential quadrature method", *Proceedings of the Institution of Mechanical Engineers, Part C: J. Mech. Eng. Sci.*, **231**(20), 3866-3885. https://doi.org/10.1177/0954406216653622

Mohammadimehr, M., Mohammadi-Dehabadi, A.A., Akhavan Alavi, S.M., Alambeigi, K., Bamdad, M., Yazdani, R. and Hanifehlou, S. (2018a), "Bending, buckling, and free vibration analyses of carbon nanotube reinforced composite beams and experimental tensile test to obtain the mechanical properties of nanocomposite", *Steel Compos. Struct., Int. J.*, **29**(3), 405-422. https://doi.org/10.12989/scs.2018.29.3.405

Mohammadimehr, M., Okhravi, S.V. and Akhavan Alavi, S.M. (2018b), "Free vibration analysis of magneto-electro-elastic cylindrical composite panel reinforced by various distributions of CNTs with considering open and closed circuits boundary conditions based on FSDT", *J. Vib. Control*, **24**(8), 1551-1569. https://doi.org/10.1177/1077546316664022

Murray, R.M. (2006), Lecture 2 - LQR Control, California Institute of Technology Control and Dynamical Systems.

Nadirian, N., Biglari, H. and Hamed, M.A. (2017), "LQG vibration control of sandwich beams with transversely flexible core equipped with piezoelectric patches", *J. Computat. Appl. Res. Mech. Eng.* (*JCARME*), **7**(1), 85-97. http://dx.doi.org/10.22061/JCARME.2017.643

Nasihatgozar, M., Khalili, S.M.R. and Fard, K.M. (2017), "General equations for free vibrations of thick doubly curved sandwich panels with compressible and incompressible core using higher order shear deformation theory", *Steel Compos. Struct., Int. J.*, **24**(2), 151-176. https://doi.org/10.12989/scs.2017.24.2.151

Nguyen, K., Thai, H.T. and Vo, T. (2015), "A refined higher-order shear deformation theory for bending, vibration and buckling analysis of functionally graded sandwich plates", *Steel Compos. Struct., Int. J.*, **18**(1), 91-120. http://dx.doi.org/10.12989/scs.2015.18.1.091

Nguyen, D.K. and Tran, T.T. (2018), "Free vibration of tapered BFGM beams using an efficient shear deformable finite element model", *Steel Compos. Struct., Int. J.*, **29**(3), 363-377. https://doi.org/10.12989/scs.2018.29.3.363

Niu, W., Zou, C., Li, B. and Wang, W. (2019), "Adaptive vibration suppression of time-varying structures with enhanced FxLMS algorithm", *Mech. Syst. Signal Process.*, **118**, 93-107. https://doi.org/10.1016/j.ymssp.2018.08.009

Qiu, Z. and Ling, D. (2014), "Finite element modeling and robust vibration control of two-hinged plate using bonded piezoelectric sensors and actuators", *Acta Mechanica Solida Sinica*, **27**(2), 146-161. https://doi.org/10.1016/S0894-9166(14)60025-2

Rajabi, J. and Mohammadimehr, M. (2019), "Bending analysis of a micro sandwich skew plate using extended Kantorovich method based on Eshelby-Mori-Tanaka approach", *Comput. Concrete, Int. J.*, **23**(5), 361-376. https://doi.org/10.12989/cac.2019.23.5.361

Rashad, M., Wahab, Mostafa M.A. and Yang, T.Y. (2019), "Experimental and numerical investigation of RC sandwich panels with helical springs under free air blast loads", *Steel Compos. Struct., Int. J.*, **30**(3), 217-230. https://doi.org/10.12989/scs.2019.30.3.217

Selim, B.A., Zhang, L.W. and Liew, K.M. (2017), "Active vibration control of CNT-reinforced composite plates with piezoelectric layers based on Reddy's higher-order shear deformation theory", *Compos. Struct.*, **163**, 350-364. https://doi.org/10.1016/j.compstruct.2016.11.011

Sharma, S., Vig, R. and Kumar, N. (2015), "Active vibration control: considering effect of electric field on PZT patches", *Smart Struct. Syst., Int. J.*, **16**(6), 1091-1105. https://doi.org/10.12989/sss.2015.16.6.1091

Shen, H.S. and Xiang, Y. (2012), "Nonlinear vibration of nanotube-reinforced composite cylindrical shells in thermal environments", *Comput. Methods Appl. Mech. Eng.*, **213-216**, 196-205. https://doi.org/10.1016/j.cma.2011.11.025

Tahouneh, V. (2017), "Vibration and mode shape analysis of sandwich panel with MWCNTs FG-reinforcement core", *Steel Compos. Struct., Int. J.*, **25**(3), 347-360. https://doi.org/10.12989/scs.2017.25.3.347

Xu, S., Cui, N., Fan, Y. and Guan, Y. (2018a), "Active vibration suppression of flexible spacecraft during attitude maneuver with actuator dynamics", *IEEE Access*, **6**, 35327-35337. https://doi.org/10.1109/ACCESS.2018.2851665

Xu, Y., Li, Z. and Guo, K. (2018b), "Active vibration robust control for FGM beams with piezoelectric layers", *Struct. Eng. Mech., Int. J.*, **67**(1), 33-43. https://doi.org/10.12989/sem.2018.67.1.033

Yazdani, R., Mohammadimehr, M. and Navi, B.R. (2019), "Free vibration of Cooper-Naghdi micro saturated porous sandwich cylindrical shells with reinforced CNT face sheets under magneto-hydro-thermo-mechanical loadings", *Struct. Eng. Mech., Int. J.*, **70**(3), 351-365. https://doi.org/10.12989/sem.2019.70.3.351

Zenkour, A.M. and Aljadani, M.H. (2018), "Mechanical buckling of functionally graded plates using a refined higher-order shear and normal deformation plate theory", *Adv. Aircraft Spacecr.*

Sci., *Int*. *J*., **5**(6), 615-632.
https://doi.org/10.12989/aas.2018.5.6.615

CC

Appendix A

$$M_c=\int_0^a\int_0^b\int_{-\frac{h_c}{2}}^{\frac{h_c}{2}}\rho_c\left(z^2\frac{\partial s}{\partial x}\frac{\partial s^T}{\partial x}+z^2\frac{\partial s}{\partial y}\frac{\partial s^T}{\partial y}+s.s^T\right)dxdydz$$

$$M_{fst}=\int_0^a\int_0^b\int_{\frac{h_c}{2}}^{\frac{h_c}{2}+h_t}\rho_{fs}\left(z^2\frac{\partial s}{\partial x}\frac{\partial s^T}{\partial x}+z^2\frac{\partial s}{\partial y}\frac{\partial s^T}{\partial y}+s.s^T\right)dxdydz$$

$$M_{fsb}=\int_0^a\int_0^b\int_{-\frac{h_c}{2}-h_b}^{-\frac{h_c}{2}}\rho_{fs}\left(z^2\frac{\partial s}{\partial x}\frac{\partial s^T}{\partial x}+z^2\frac{\partial s}{\partial y}\frac{\partial s^T}{\partial y}+s.s^T\right)dxdydz$$

$$M_{pzs_t}=\sum_{i=1}^{N_{pz}}\int_0^a\int_0^b\int_{\frac{h_c}{2}+h_t}^{\frac{h_c}{2}+h_t+h_{pz_i}}\rho_{pzs_i}\left(z^2\frac{\partial s}{\partial x}\frac{\partial s^T}{\partial x}+z^2\frac{\partial s}{\partial y}\frac{\partial s^T}{\partial y}+s.s^T\right)dxdydz$$

$$M_{pzs_b}=\sum_{i=1}^{N_{pz}}\int_0^a\int_0^b\int_{-\frac{h_c}{2}-h_b-h_{pz_i}}^{-\frac{h_c}{2}-h_b}\rho_{pzs_i}\left(z^2\frac{\partial s}{\partial x}\frac{\partial s^T}{\partial x}+z^2\frac{\partial s}{\partial y}\frac{\partial s^T}{\partial y}+s.s^T\right)dxdydz$$

$$M_{pza_t}=\sum_{i=1}^{N_{pz}}\int_0^a\int_0^b\int_{\frac{h_c}{2}+h_t}^{\frac{h_c}{2}+h_t+h_{pz_i}}\rho_{pza_i}\left(z^2\frac{\partial s}{\partial x}\frac{\partial s^T}{\partial x}+z^2\frac{\partial s}{\partial y}\frac{\partial s^T}{\partial y}+s.s^T\right)dxdydz$$

$$M_{pza_b}=\sum_{i=1}^{N_{pz}}\int_0^a\int_0^b\int_{-\frac{h_c}{2}-h_b-h_{pz_i}}^{-\frac{h_c}{2}-h_b}\rho_{pza_i}\left(z^2\frac{\partial s}{\partial x}\frac{\partial s^T}{\partial x}+z^2\frac{\partial s}{\partial y}\frac{\partial s^T}{\partial y}+s.s^T\right)dxdydz$$

Appendix B

$$\varepsilon^T\boldsymbol{\sigma}=\begin{bmatrix}\varepsilon_{xx} & \varepsilon_{yy} & \gamma_{xy} & \gamma_{yz} & \gamma_{xz}\end{bmatrix}\begin{bmatrix}\sigma_{xx}\\ \sigma_{yy}\\ \sigma_{xy}\\ \sigma_{yz}\\ \sigma_{xz}\end{bmatrix}=\varepsilon_{xx}\sigma_{xx}+\varepsilon_{yy}\sigma_{yy}+\gamma_{xy}\sigma_{xy}+\gamma_{yz}\sigma_{yz}+\gamma_{xz}\sigma_{xz}$$

$$=Q_{11}\varepsilon_{xx}^2+Q_{22}\varepsilon_{yy}^2+2Q_{12}\varepsilon_{xx}\varepsilon_{yy}+Q_{66}{\gamma_{xy}}^2+Q_{55}{\gamma_{xz}}^2+Q_{44}{\gamma_{yz}}^2$$

$$=Q_{11}\left(-z\frac{\partial^2 w}{\partial x^2}\right)^2+Q_{22}\left(-z\frac{\partial^2 w}{\partial y^2}\right)^2+2Q_{12}\left(-z\frac{\partial^2 w}{\partial x^2}\right)^T\left(-z\frac{\partial^2 w}{\partial y^2}\right)+Q_{66}\left(-2z\frac{\partial^2 w}{\partial x\partial y}\right)^2$$

$$\varepsilon^T\boldsymbol{\sigma}=Q_{11}\left(z^2\left(\frac{\partial^2 w}{\partial x^2}\right)^T\left(\frac{\partial^2 w}{\partial x^2}\right)\right)+Q_{22}\left(z^2\left(\frac{\partial^2 w}{\partial y^2}\right)^T\left(\frac{\partial^2 w}{\partial y^2}\right)\right)+2Q_{12}\left(z^2\left(\frac{\partial^2 w}{\partial x^2}\right)^T\left(\frac{\partial^2 w}{\partial y^2}\right)\right)+Q_{66}\left(4z^2\left(\frac{\partial^2 w}{\partial x\partial y}\right)^T\left(\frac{\partial^2 w}{\partial x\partial y}\right)\right)$$

$$\varepsilon^T\boldsymbol{\sigma}=Q_{11}\left(\Psi^T z^2\frac{\partial^2 s}{\partial x^2}\frac{\partial^2 s}{\partial x^2}^T\Psi\right)+Q_{22}\left(\Psi^T z^2\frac{\partial^2 s}{\partial y^2}\frac{\partial^2 s}{\partial y^2}^T\Psi\right)+2Q_{12}\left(\Psi^T z^2\frac{\partial^2 s}{\partial x^2}\frac{\partial^2 s}{\partial y^2}^T\Psi\right)+Q_{66}\left(\Psi^T 4z^2\frac{\partial^2 s}{\partial x\partial y}\frac{\partial^2 s}{\partial x\partial y}^T\Psi\right)$$

$$\varepsilon^T\boldsymbol{\sigma}=\Psi^T(Q_{11}\left(z^2\frac{\partial^2 s}{\partial x^2}\frac{\partial^2 s}{\partial x^2}^T\right)+Q_{22}\left(z^2\frac{\partial^2 s}{\partial y^2}\frac{\partial^2 s}{\partial y^2}^T\right)+2Q_{12}\left(z^2\frac{\partial^2 s}{\partial x^2}\frac{\partial^2 s}{\partial y^2}^T\right)+Q_{66}\left(4z^2\frac{\partial^2 s}{\partial x\partial y}\frac{\partial^2 s}{\partial x\partial y}^T\right))\Psi$$

Appendix C

$$U_{fst}=\frac{1}{2}\int_0^a\int_0^b\int_{\frac{h_c}{2}}^{\frac{h_c}{2}+h_t}\varepsilon^T\sigma_{fs\text{-}t}dxdydz=\frac{1}{2}\Psi^T K_{fs\text{-}t}\Psi$$

$$K_{fst}=\int_0^a\int_0^b\int_{\frac{h_c}{2}}^{\frac{h_c}{2}+h_t}(Q_{11f}\left(z^2\frac{\partial^2 s}{\partial x^2}\frac{\partial^2 s}{\partial x^2}^T\right)+Q_{22f}\left(z^2\frac{\partial^2 s}{\partial y^2}\frac{\partial^2 s}{\partial y^2}^T\right)+2Q_{12f}\left(z^2\frac{\partial^2 s}{\partial x^2}\frac{\partial^2 s}{\partial y^2}^T\right)+Q_{66f}\left(4z^2\frac{\partial^2 s}{\partial x\partial y}\frac{\partial^2 s}{\partial x\partial y}^T\right))dxdydz$$

$$U_{fsb}=\frac{1}{2}\int_0^a\int_0^b\int_{-\frac{h_c}{2}-h_b}^{-\frac{h_c}{2}}\varepsilon^T\sigma_{fs\text{-}b}dxdydz=\frac{1}{2}\Psi^T K_{fs\text{-}b}\Psi$$

$$K_{fsb}=\int_0^a\int_0^b\int_{-\frac{h_c}{2}-h_b}^{-\frac{h_c}{2}}(Q_{11f}\left(z^2\frac{\partial^2 s}{\partial x^2}\frac{\partial^2 s}{\partial x^2}^T\right)+Q_{22f}\left(z^2\frac{\partial^2 s}{\partial y^2}\frac{\partial^2 s}{\partial y^2}^T\right)+2Q_{12f}\left(z^2\frac{\partial^2 s}{\partial x^2}\frac{\partial^2 s}{\partial y^2}^T\right)+Q_{66f}\left(4z^2\frac{\partial^2 s}{\partial x\partial y}\frac{\partial^2 s}{\partial x\partial y}^T\right))dxdydz$$